ELSEVIER

Powder Technology 97 (1998) 26–34

POWDER TECHNOLOGY

Effect of shear schedule on particle size, density, and structure during flocculation in stirred tanks

Patrick T. Spicer [a], Sotiris E. Pratsinis [a,*], Judy Raper [b], Rose Amal [b], Graeme Bushell [b], Gabrie Meesters [c]

[a] *Department of Chemical Engineering, University of Cincinnati, 697 Rhodes Hall, PO Box 210171, Cincinnati, OH 45221-0171, USA*
[b] *School of Chemical Engineering and Industrial Chemistry, University of New South Wales, Kensington, NSW 2052, Australia*
[c] *Gist-Brocades B.V., 2600 MA Delft, The Netherlands*

Received 20 December 1996; revised 11 September 1997

Abstract

The effect of shear history on the evolution of the polystyrene–alum floc size, density, and structure is investigated by small-angle light scattering during cycled-shear and tapered-shear flocculation in a stirred tank using a Rushton impeller. First, various sampling schemes are experimentally evaluated. The floc structure is characterized by the mass fractal dimension, D_f, and the relative floc density. During turbulent shear flocculation, small floc structures are shown to be more open ($D_f = 2.1$) than larger floc structures ($D_f = 2.5$) as a result of shear-induced restructuring during steady state attainment. Flocs produced by cycled-shear flocculation are grown at shear rate $G = 50\ s^{-1}$ for 30 min, are fragmented at $G_b = 100$, 300, or 500 s^{-1} for one minute, and then are regrown at $G = 50\ s^{-1}$. This shear schedule decreases the floc size but compacts the floc structure. When flocs are produced by gradual reduction of the shear rate from $G = 300$ to $50\ s^{-1}$ (tapered-shear flocculation), smaller though equally dense flocs are produced compared with cycled-shear flocculation. The cycled-shear flocculation method produces the largest flocs with the highest potential for sedimentation when the fragmentation shear rate is $G_b = 300\ s^{-1}$.

Keywords: Floc structure; Shear induced flocculation; Fractal dimensions; Cycled shear; Sedimentation

1. Introduction

The recovery/removal of suspended fine particles is essential to water treatment, materials processing, and production of biological commodities like detergent enzymes. Typical solid–liquid separation processes begin with flocculation, the shear-induced collision of destabilized suspended fine particles to form larger flocs that are more easily removed by sedimentation, filtration, and/or centrifugation. Particle collision (coagulation) occurs by the relative motion of particles in the fluid shear field, but, as the flocs (particles) grow larger, fluid shear stresses can also break the flocs into smaller fragments (fragmentation). The evolution of the floc size distribution during flocculation is accompanied by changes in the floc structure as well. As fine primary particles combine to form flocs, they become irregular structures incorporating increasing amounts of interstitial water [1]. Conversely, when flocs break by applied shear, they tend to do so at the weakest points in the floc structure. This produces fragments that are stronger and more compact but smaller than the parent floc [2]. Thus, coagulation increases the average floc size, but decreases its average compactness, while fragmentation decreases the average floc size and increases the average floc compactness. The optimization of a flocculation process therefore depends on the relative rates of coagulation and fragmentation.

After a characteristic time of shear-induced flocculation, a steady state is reached between coagulation and fragmentation and the floc size distribution no longer changes [3]. More recently, it has been shown that this steady state size distribution, scaled with the average floc size, does not depend on the applied shear rate [4,5]. A change in the applied shear rate drives a suspension at steady state to a new steady state. By lowering or raising the shear rate, larger or smaller flocs, respectively, are formed. After the second steady state has been attained, if the original shear rate is then re-applied, two types of behavior have been observed experimentally: reversible and irreversible. For particle suspen-

* Corresponding author. Tel.: +1 513 556 2761; Fax: +1 513 556 3473

0032-5910/98/$19.00
PII S0032-5910(97)03389-5

sions destabilized with an ionic salt (i.e. NaCl), when the original shear rate is re-applied, the steady state average floc size returns to its original steady state value. These suspensions exhibit reversible floc dynamics because floc fragmentation and regrowth does not affect the van der Waals binding forces between primary particles [6]. Current flocculation models agree with these data, indicating that the steady state floc size distribution (FSD) for reversible systems is independent of initial conditions [7].

When the flocculant is a precipitated solid (i.e. $Al(OH)_3$) or polymer, the suspension exhibits irreversible floc dynamics. Francois [8] studied kaolin–$Al(OH)_3$ floc fragmentation and regrowth at various shear rates in stirred tanks. In all cases, flocs regrew but did not attain their previous steady state average size. He explained this as floc formation by a multilevel progression: primary particles combined to form dense microflocs, which in turn combined to form the next level and so on. Leu and Ghosh [9] flocculated kaolin suspensions with a polyelectrolyte and observed a similar behavior: flocs were reformed after intense fragmentation but did not attain their original steady state average size. They attributed this to the detachment of polymer chains from kaolin particles, resulting in a reduced collision efficiency and, thus, smaller particles. Clark and Flora [10] studied cycled-shear flocculation of polystyrene–$Al(OH)_3$ flocs by analysis of floc microphotographs. The flocs, formed at $G_f = 35\ s^{-1}$, fragmented at $G_b = 150$–$1800\ s^{-1}$ and re-formed at $G_r = 35\ s^{-1}$, exhibited increasingly compact structures but no clear size variation trend was observed. Glasgow and Liu [11] found that kaolin–polymer flocs were more dense following cycled-shear flocculation with cycled introduction of additional flocculant.

The irreversibility of aggregates during cycled shear is most likely the result of particle–flocculant bond breakage during fragmentation. Once broken, these bonds are not able to re-form to their previous extent, reducing the efficiency of subsequent aggregate–aggregate collisions [9]. Extensive simulations indicate that a reduction in the collision efficiency of aggregates produces more compact, smaller structures relative to the case when collisions are 100% successful. This results from the need for the colliding aggregates to interpenetrate further than before if successful collisions are to occur [10,12]. Thus, intense shearing produces fragmentation which, by breaking particle–flocculant bonds, in turn reduces the 'stickiness' of the resulting fragments. As a result, the efficiency of subsequent collisions is reduced and smaller, more compact aggregate structures are produced by these collisions.

Any shearing of irregular flocs is likely to produce compaction as particle–particle bonds shift to positions with higher coordination numbers. This can happen even when fragmentation does not occur; numerical simulations of this process produced a change in aggregate fractal dimension, D_f, from 1.89 to 2.13 [13]. Shear-induced coagulation simulations excluding any restructuring produce fractal clusters with $D_f = 1.8$ [14], while experimental shear-induced coagulation–fragmentation processes produce small aggregates with $D_f = 2.1$ and large aggregates with $D_f = 2.5$ [15,16]. The shift from $D_f = 1.8$ to 2.1 probably results from shear-induced reorganization while the shift from $D_f = 2.1$ to 2.5 is likely brought about by more intense restructuring during fragmentation–regrowth cycles that occur as the larger aggregates interact more with the small eddies. As aggregates pass through regions of high and low shear rates in a stirred tank, reorganization and restructuring can both occur. Restructuring is likely the most prevalent compaction mechanism when a steady state is reached between coagulation and fragmentation during flocculation. As a result, the deliberate application of a cycled shear schedule is an excellent way to study the incidental long-term microscopic aging effects brought about by many passes of aggregates through the high shear impeller region of a stirred tank. This is because intentionally higher shear rates reduce the Kolmogorov microscale to the extent that most particles are fragmented and the cycled-shear effect is more homogeneous.

Irreversible flocculation offers a simple method of increasing floc compactness and suggests that some degree of floc fragmentation by fluid shear may not always be undesirable. In addition, this type of cycling of the average floc structure has been shown to have profound effects on the viscosity of more concentrated suspensions [17–20]. As a result, it is of interest to accurately characterize floc compaction and determine the best means of bringing it about.

The objective of this work is to use small-angle light scattering to study the size and structural dynamics of polystyrene–alum flocs. Three sampling techniques of the floc size distribution are evaluated. The evolution of the floc size distribution under various shear schedules is presented. The evolution of the floc structure is presented using the floc mass fractal dimension, D_f, and the average relative floc density is used to characterize the floc removal rates. The characteristics of flocs produced by cycled-shear flocculation are compared with those made by tapered-shear flocculation, a technique often applied in water treatment.

2. Experimental

Flocculation of an aqueous suspension of monodisperse, spherical, polystyrene particles (primary particle size $d_0 = 0.87\ \mu m$) was studied in a 2.8 liter, baffled, stirred tank [5]. The suspension was mixed using a radial flow (Rushton) Lightnin R100 impeller. The center of the impeller was positioned at 1/3 the height of the tank. The solids volume fraction was $\phi = 1.4 \times 10^{-5}$, corresponding to an initial particle number concentration of $4 \times 10^7\ cm^{-3}$. The flocculant was aluminum sulfate hydrate ($Al_2(SO_4)_3 16H_2O$; Aldrich, 98%) [5,10]. All experiments were conducted using a constant $Al_2(SO_4)_3 16H_2O$ concentration of 10 mg/l. Sodium hydrogen carbonate ($NaHCO_3$; Aldrich, 99%) at a concentration of 1 mM was used to buffer the suspension and the pH was kept at 7.2 ± 0.05 during all experiments.

The average turbulent shear rate within the stirred tank was characterized using the spatially averaged velocity gradient G. The polystyrene suspension was first mixed at $G=300$ s^{-1} for 5 minutes to break up any agglomerates. The flocculant was then added and mixed with the suspension for 1 minute. The impeller was then set to the desired speed (100 rpm for $G=50$ s^{-1}, $G_{max}=597$ s^{-1}; 156 rpm for $G=100$ s^{-1}, $G_{max}=1183$ s^{-1}; 248 rpm for $G=200$ s^{-1}, $G_{max}=2371$ s^{-1}; 325 rpm for $G=300$ s^{-1}, $G_{max}=3556$ s^{-1}; 460 rpm for $G=500$ s^{-1}, $G_{max}=5969$ s^{-1}), where the volume averaged shear rate G and its maximum, G_{max}, are calculated using a power number, $N_p=5$, and the characteristic fluid volume (tank volume for G or impeller swept volume for G_{max}) following the procedures of Spicer and Pratsinis [5]. The impeller speeds for flocculation were chosen to eliminate floc sedimentation and to produce floc structures unaffected by the sampling procedure. The impeller rotational velocity was measured using an optical tachometer (Ono Sokki HT-4100) and varied by less than 1 rpm. All experiments were carried out 2–3 times and very little variation was observed.

The floc sampling technique is crucial to accurately characterize flocculation dynamics. A large number of particles (>500) must be sampled to accurately determine a floc size distribution, while care must be taken not to alter fragile floc structures by sampling/removal procedures. Samples were obtained for analysis by one of three techniques: (1) withdrawal of a sample to be placed into the sample cell of the light scattering instrument using a 5 mm i.d. pipette [5,11]; (2) withdrawal of a sample into the flow-through sample cell using a syringe [20,21]; (3) continuous recycle of the suspension through the sample cell using a peristaltic pump (Gilson Minipuls) [15]. In the case of the peristaltic pump, the suspension passed through 6 mm i.d. rubber tubing at a flow rate of 3 cm^3/s ($Re=618$), while for the syringe pump the flow rates were much lower. The pump was located upstream of the particle analyzer sample cell to prevent shearing of the aggregates in the pinch portion of the pump prior to size measurement. In addition, the results in Fig. 1 compare the size data for samples taken by all three methods. For all three sampling techniques, samples were withdrawn from the same location in the tank, midway between the impeller and the top of the suspension. This is the location of the recirculation zone for a radial flow impeller like the Rushton and will provide an accurate sampling of the bulk of the stirred tank [5,6,10].

Small-angle light scattering measurements by a Malvern Mastersizer E (Malvern Instruments) were used to evaluate the floc size distribution and the average floc structure and density as a function of time. The structure of the flocs was determined quantitatively by their mass fractal dimension, D_f, a measure of the floc compactness that varies from 1, for a floc made of a line of particles, to 3, for a compact spherical-shaped floc of primary particles [23]. The mass of a fractal floc varies with its characteristic length l as

$$M \propto l^{D_f} \tag{1}$$

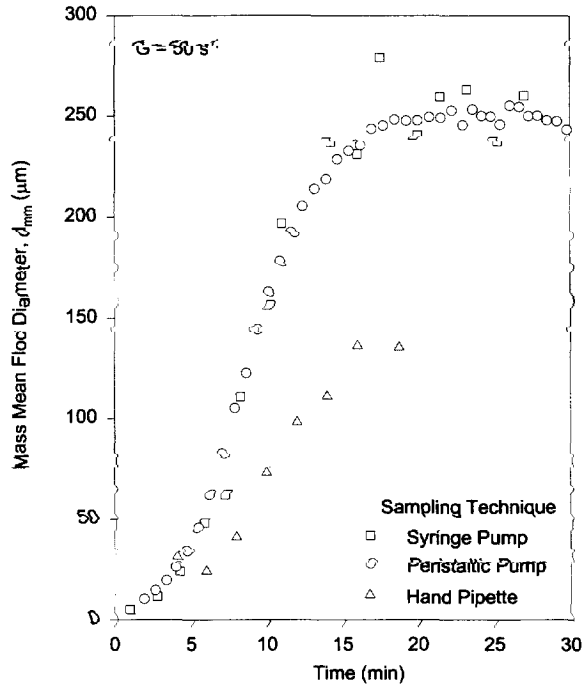

Fig. 1. Comparison of the effect of three sampling techniques on the evolution of the mass mean diameter d_{mm} of polystyrene–alum flocs at $G=50$ s^{-1} and $\phi=1.4\times10^{-5}$. Using the hand pipette results in smaller flocs.

The scattering behavior of suspended particles is dependent on the ratio of primary particle size, d_0, to the wavelength of light scattered, λ, so that if

$$d_0 \gg \lambda \tag{2}$$

the fractal dimension D_f is determined from the slope ($m=D_f-3$) of a log–log plot of the ratio of the initial suspended particle volume fraction ϕ_p to that of the flocculated suspension, ϕ_f, versus the mass mean diameter d_{mm} of the floc size distribution based on rearrangement of Eq. (1) [15,16]:

$$\frac{\phi_p}{\phi_f} \propto d_{mm}^{D_f-3} \tag{3}$$

The apparent volume fraction of the suspended flocs is a function of the obscuration, OB, of the laser beam, a parameter reported by the Mastersizer E [6,16]:

$$\phi_f = \frac{d_{sm}\ln(1-OB)}{3L} \tag{4}$$

where d_{sm} is the Sauter mean diameter of the size distribution [16] and L is the laser path length (2.1 mm). This technique of floc structure characterization allows measurement of the average floc fractal dimension by averaging the floc structure over the duration of the experiment. Characterization of floc restructuring is also possible when multiple slopes occur [15].

For flocs composed of primary particles smaller than the wavelength of scattered light (i.e. the opposite condition of Eq. (2)), the fractal dimension D_f can be determined from

the negative slope of a log–log plot of the light intensity scattered by the floc, $I(Q)$, as a function of the wavenumber used, Q (the magnitude of the difference between the incident and scattered wave vectors):

$$I \propto Q^{-D_f} \tag{5}$$

This technique of floc structure characterization allows instantaneous measurement of the average floc fractal dimension and thus its evolution with time [21,22,24,25].

In this study, the primary particles making up the flocs have a diameter of 0.87 μm, while the wavelength of laser light is 0.475 μm. Because of the size similarity, the results of both structural analyses have been used and compared to best represent the particle dynamics under study. It should be noted that the technique summarized by Eqs. (2)–(4) has the most technical validity because of the superior size of the employed primary particles relative to the laser wavelength.

3. Results and discussion

3.1. Floc size distributions

First, the three sampling techniques were compared to select the one introducing the least bias. Fig. 1 shows a comparison of the evolution of the mass mean floc diameter d_{mm} as a function of time for flocculation of polystyrene particles with 10 mg/l of $Al_2(SO_4)_3 16H_2O$ at a spatially averaged shear rate of $G = 50\ s^{-1}$. Clearly, flocculation increases the average particle size until it reaches a steady state value around 250 μm. In Fig. 1 the data sampled by the syringe and by the peristaltic pump fall on top of one another despite the difference in flow rates, indicating the lack of any shear effects for these techniques. Since the syringe method exposes the aggregates to a much lower shear rate, one would expect a positive deviation by the pump data (relative to the syringe data) if the pump were inducing additional flocculation and a negative deviation if the pump were fragmenting the flocs. Since no such trend is observed, it is reasonable to conclude that the pump is not altering the floc size distribution. The samples taken by hand pipette, however, produced significantly smaller flocs than the other two techniques, though the hand pipette data qualitatively follow the pump data. This may result from floc fragmentation during transfer from the pipette to the sample cell or, more likely, by floc settling in the time between sampling and analysis. The peristaltic pump was used in all subsequent experiments because of the large number of samples possible and the limited sampling bias.

The evolution of the normalized floc size distribution for $G = 50\ s^{-1}$ is shown in Fig. 2 corresponding to the conditions in Fig. 1. Initially, coagulation dominates and the primary particles rapidly collide and grow. Once flocculation has begun, the particle size distribution evolves rapidly from monodispersity by broadening into larger sizes as particle collisions form flocs. After only 2 minutes, the floc size distribution has formed a second mode around 10 μm in addition to the primary particle mode at about 1 μm. The primary particle mode is depleted by collisions with the larger flocs and the larger mode grows further. This is in agreement with theoretical studies of laminar [4,15] and turbulent shear-induced flocculation [5,6]. After 20 min, the floc size distribution no longer changes significantly, indicating that a steady state has been attained between coagulation and fragmentation, as indicated by Fig. 1 as well. It is now of interest to force the floc size distribution to deviate from its dynamic steady state in order to characterize its reversibility.

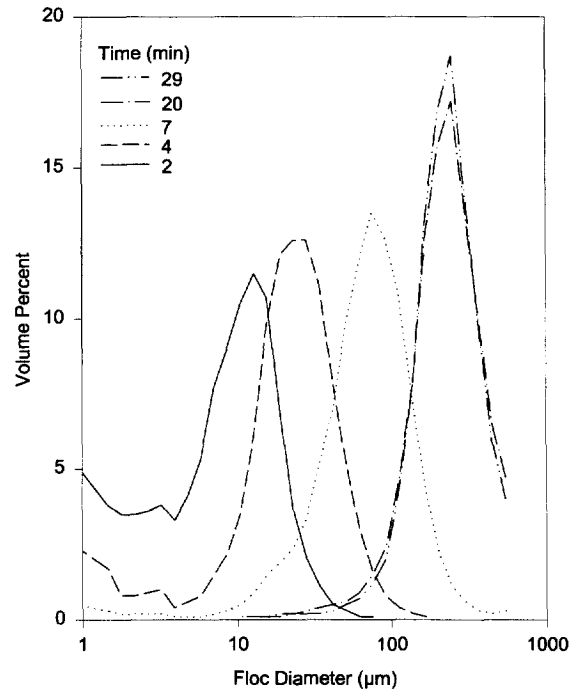

Fig. 2. Evolution of the polystyrene–alum floc size distribution (FSD) for $G = 50\ s^{-1}$ and $\phi = 1.4 \times 10^{-5}$. The FSD broadens into the larger sizes and becomes fully developed as the primary particles are depleted and a steady state is reached between coagulation and fragmentation.

Fig. 3 shows the evolution of d_{mm} during three flocculation cycles of initially constant shear at $G_f = 50\ s^{-1}$ for 30 minutes, fragmentation for 1 minute at $G_b = 100$, 300, or 500 s^{-1}, and again at $G_r = 50\ s^{-1}$ for 30 minutes to re-form (regrow) the flocs. Incidentally, the flocculation curves prior to $t = 30$ min indicate the reproducibility of the process. As was shown in Fig. 2, the particle size increases rapidly while coagulation dominates at early times. At 30 min, d_{mm} drops immediately to a minimum value during the fragmentation period. The higher G_b, the lower the minimum value of d_{mm} as a result of the increased fragmentation rate. After 1 minute of fragmentation, as the shear rate is returned to $G_r = 50\ s^{-1}$, d_{mm} grows to a new steady state value. In Fig. 3, this new steady state average floc size is 200, 175, and 150 μm for G_b equal to 100, 300, and 500 s^{-1}, respectively. This is significantly lower than the original one, $d_{mm} = 250$ μm at $t \leq 30$ min, indicating that the employed suspension exhibits irreversible behavior [8–11].

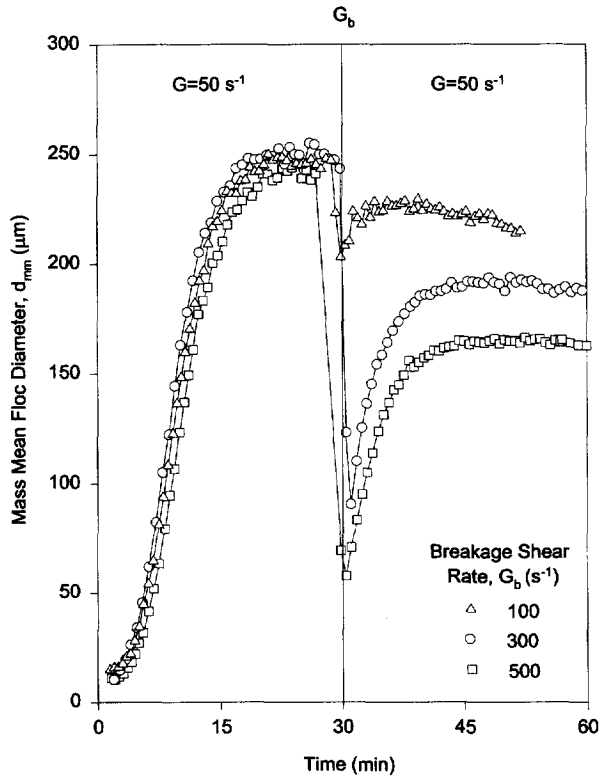

Fig. 3. Effect of cycled-shear on the evolution of d_{mm}. Increasing the fragmentation shear rate G_b for 1 minute decreases the size of fragments produced and the final floc size attained.

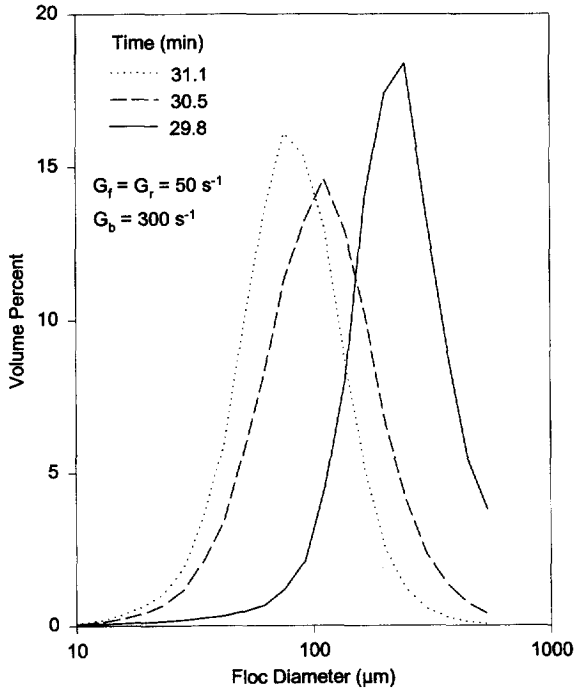

Fig. 4. Snapshots of the floc size distribution (FSD) during intense shear, $G_b = 300\ s^{-1}$, for 1 minute. The FSD shifts into smaller sizes by the increased fragmentation rates.

Fig. 4 shows the dynamics of the floc size distribution (FSD) during the above cycled-shear flocculation with $G_b = 300\ s^{-1}$. Just before the intense shearing at 29.8 min the floc size distribution is at a steady state centered around 250 μm. After this point, however, increasing the shear rate to $300\ s^{-1}$ increases the floc fragmentation rate and at 30.5 min the distribution is broader and centered around 100 μm. A few seconds later, at the completion of the intense shearing step, the distribution has narrowed a bit more and centers around 90 μm and the average floc size is at its minimum (Fig. 3). Comparison of the FSD at 29.8 and 31.1 min indicates that significant fragmentation has occurred. In 1 minute the majority of the FSD has been shifted into a smaller size range which is similar to the FSD observed at $t = 7$ min (Fig. 2).

3.2. Floc density and structure

Fig. 5 shows the average relative floc density, ϕ_p/ϕ_f, of polystyrene–alum aggregates flocculated at $G = 50\ s^{-1}$ plotted as a function of the mass mean floc diameter for the first 15 minutes of flocculation. At this early stage, the density decreases rapidly with increasing floc size, indicating the presence of increasingly open structures during coagulation ($t \leq 15$ min), in agreement with the study of Kusters et al. [16] on aggregates smaller than 20 μm. The two regions of linearity of the data indicate that the smaller flocs possess a fractal-like structure with $D_f = 2.1 \pm 0.05$, while larger flocs possess a fractal dimension of $D_f = 2.5 \pm 0.05$. This deviation at large sizes is the result of shear-induced compaction that occurs as the flocs become larger and more susceptible to fragmentation and regrowth. The two values of D_f found here for turbulent shear-induced flocculation are identical to those found by Oles [15] for laminar shear-induced flocculation, indicating that the mechanism of floc structure formation is

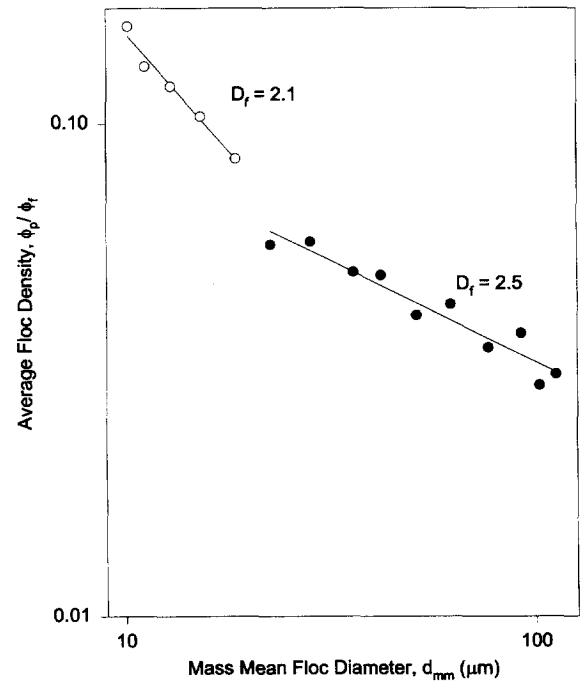

Fig. 5. Determination of the average floc mass fractal dimension D_f from the slope of a log–log plot of the average floc density as a function of d_{mm} [15].

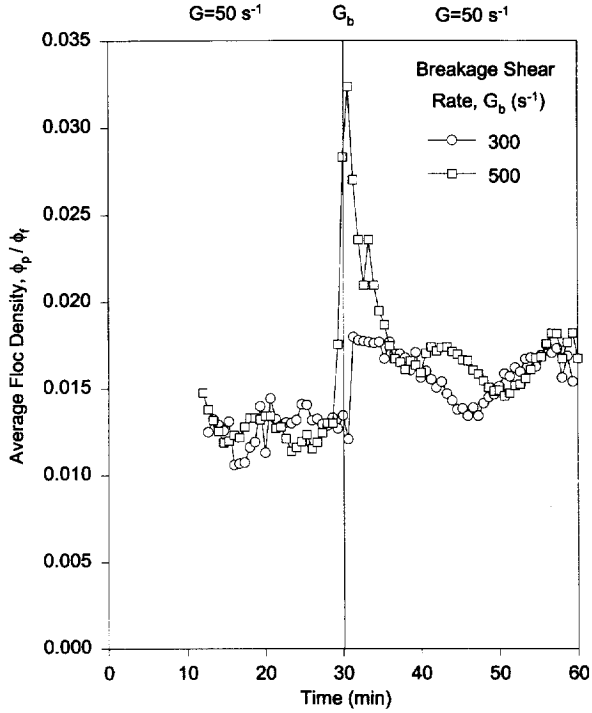

Fig. 6. Effect of cycled-shear flocculation on the average floc density. Application of $G_b = 300$ or $500\ s^{-1}$ increases the density of the fragments produced and the new steady state density following regrowth.

similar, despite the different flow fields. The determination of D_f by Eq. (3) does not allow a rigorous characterization of the effect of cycled-shear flocculation on the evolution of the floc structure because of the small range of sizes over which regrowth of the flocs occurs. However, by plotting the dimensionless average floc density, ϕ_p/ϕ_f, as a function of time, it is possible to assess the effects of cycled-shear flocculation on floc density and apparent removal rate.

Fig. 6 shows the evolution of the relative average floc density for the employed shear cycles (e.g. Fig. 3). After the initial stage ($t < 10$ min) of decreasing density shown in Fig. 5, the density levels off at a steady state value as coagulation and fragmentation balance one another in Fig. 6. At 30 min, the intense shearing causes a significant increase in the average floc density, as a larger G_b produces relatively denser fragments during fragmentation, in agreement with the current understanding that flocs break preferentially at weak points and form more compact fragments [2]. Once the intense shearing ceases and $G_r = 50\ s^{-1}$ is applied, the density drops significantly to a minimum value, indicating an increased openness of the floc structure as the flocs re-form, and then the density increases by shear-induced restructuring. This restructuring is the result of aggregate flow through the impeller region of the stirred tank, where the aggregate structure is compacted to more dense forms by shear-induced reorganization or fragmentation and subsequent regrowth. These results are in qualitative agreement with those of Spicer et al. [26] who found by image analysis a similar increase in floc compaction after steady state had been attained as a result of shear-induced floc restructuring. As in Fig. 3 for d_{mm}, the new steady state floc density is different (larger) than the original steady state value, indicating that more compact structures are produced by cycled-shear flocculation. This is observed for the two highest G_b, as the obscuration data for $G_b = 100\ s^{-1}$ had not been recorded. Increasing the G_b from 300 to 500 s^{-1} produces little change of the steady state density.

Another method of evaluating the evolution of the floc structure is to plot the log of the scattered light intensity, $I(Q)$, as a function of the log of the light wavenumber, Q (Fig. 7). Fig. 7 shows such data for the polystyrene–alum flocs after 10 minutes of flocculation at $G = 50\ s^{-1}$. The linear region indicates a fractal scaling of mass within the aggregate, allowing the extraction of a mass fractal dimension (from the negative slope of the plot) averaged over the entire floc size distribution at each sample time instead of averaged over the entire experiment as in Fig. 5. Where Fig. 5 indicates the fractal dimension for a block of time during the experiment, determination of the slope of the log I versus log Q plots allows one to plot an average D_f as a function of time to monitor the aggregate structural dynamics throughout the experiment (Fig. 8).

Fig. 8 shows the evolution of the average mass fractal dimension, D_f, for the same conditions as in Fig. 3, Fig. 5, and Fig. 6. The average floc structure attains a steady state value around 2.25 after 15 minutes, with a gradual increase to 2.3 (indicating compaction) as a result of shear-induced restructuring. This $D_f = 2.3$ is in excellent agreement with the average of the values $D_f = 2.1$ and 2.5 found in Fig. 5 and the compaction indicated by the increased floc density in Fig. 6 after 15 minutes. As in Fig. 6, when fragmentation is momen-

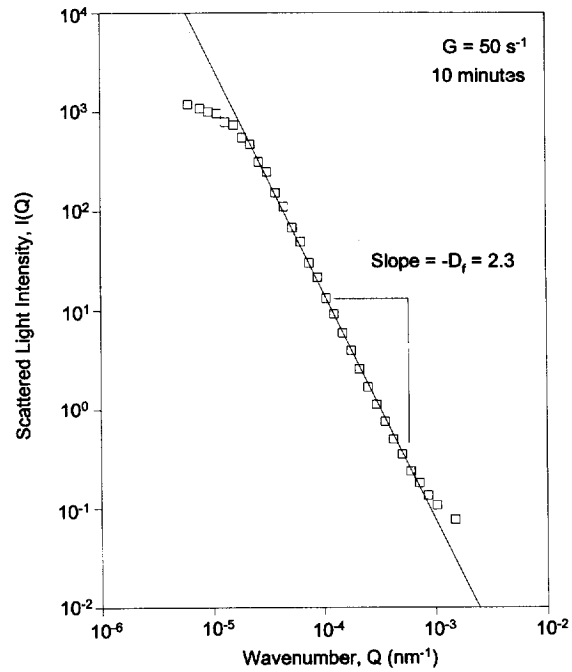

Fig. 7. Determination of the average floc mass fractal dimension D_f from the negative slope of a log–log plot of the scattered light intensity as a function of wavenumber [24,25].

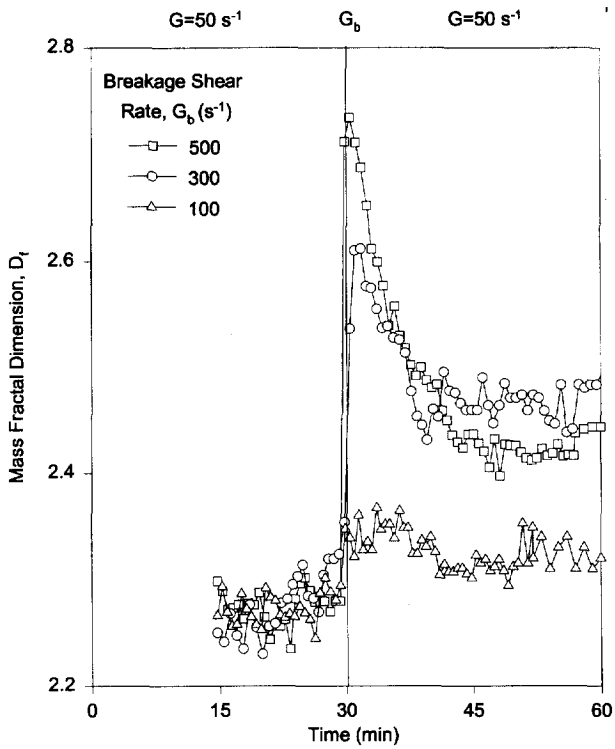

Fig. 8. Effect of cycled-shear flocculation on the average floc mass fractal dimension D_f. An increase in G_b increases the D_f of the fragments produced by preferential fragmentation and the new steady state D_f by altering the particle–particle bonds.

tarily induced by an increased shear rate at 30 min, the average D_f increases significantly as more compact floc structures are produced by fragmentation. Increasing the fragmentation shear rate increases the fragmentation rate and produces more compact structures relative to the lower fragmentation shear rates. Following the fragmentation step, when G is returned to 50 s^{-1}, a new steady state D_f is reached for all three fragmentation shear rates, each one larger (indicating the formation of more compact structures) than the pre-fragmentation value. At the lowest G_b (100 s^{-1}), there is only a slight increase in D_f following aggregate re-formation, while there is little distinction between $G_b = 300$ and 500 s^{-1} within experimental variation. Once again, the post-fragmentation results in Fig. 8 are in excellent agreement with the density data in Fig. 6, indicating the validity of this type of analysis even for particles outside of the strict range of validity of this analysis. This technique has also been successfully applied to characterize aggregates of kaolin composed of particles larger than the laser wavelength [21,22,24,25].

3.3. Practical implications

The results in Figs. 3, 6 and 8 indicate that a brief step increase in the applied shear rate can produce slightly smaller but more compact flocs. This may have some interesting implications in floc removal from suspensions since this is the primary goal of using flocculation in most chemical processes. As the goal is usually to make large and compact flocs, an optimal shear rate schedule may exist with respect to floc sedimentation. Thus, it is useful to compare the above cycled-shear flocculation method with more traditional methods.

The concept of tapered-shear flocculation, the gradual reduction of the applied shear rate in order to minimize fragmentation but maximize mixing and particle collisions, has been used to improve flocculation performance. In theory, tapered-shear flocculation should perfectly exploit floc irreversibilities because it seeks to form flocs from compact microflocs versus the open structures resulting from conventional constant-shear flocculation.

Fig. 9 shows the evolution of d_{mm} during a typical tapered-shear flocculation experiment using four shear rates ($G_1 = 300$ s^{-1}, $G_2 = 200$ s^{-1}, $G_3 = 100$ s^{-1}, $G_4 = 50$ s^{-1}) applied for 15 minutes each. Initially, the same type of behavior seen in Fig. 3 is observed: a rapid initial growth rate as particle collisions increase the average floc size. After about 5 minutes, floc growth slows down and the average floc size reaches a steady state value much faster than in Fig. 3 as the applied shear rate is much larger. d_{mm} begins to decrease as a result of the combination of floc compaction by the strong shear forces [26] and the heterogeneous flow conditions of the stirred tank [27]. When G is reduced to 200 s^{-1}, after 15 minutes, the average floc size increases immediately to level off at about 60 μm. At 30 minutes, further reduction of G to 100 s^{-1} causes another increase in floc size to about 75 μm. Finally, at 45 minutes, reduction of the shear rate to 50 s^{-1} further increases d_{mm} to a final steady state value of about 110 μm, which is less than half of the steady state d_{mm} reached

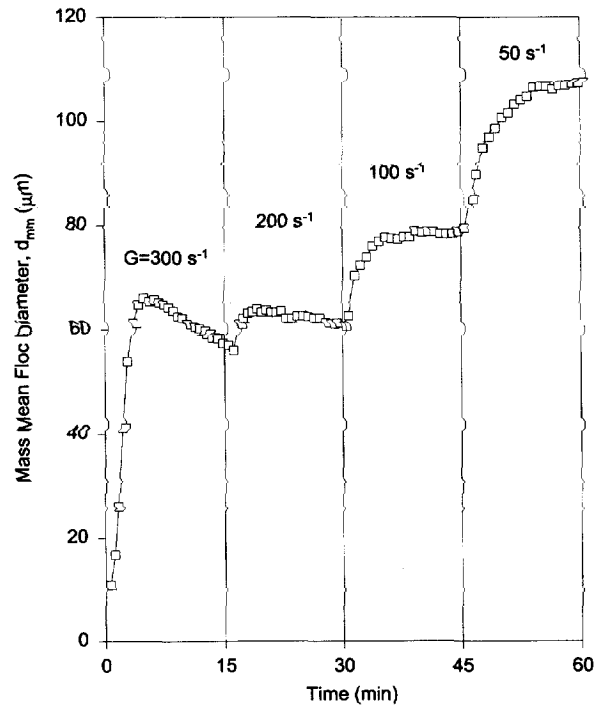

Fig. 9. Evolution of d_{mm} during tapered-shear flocculation. Initially the floc size increases during rapid coagulation, reaches a maximum ($t = 5$ min), and then decreases as restructuring occurs. As the shear rate is reduced, the floc size increases to a new steady state at each new shear rate.

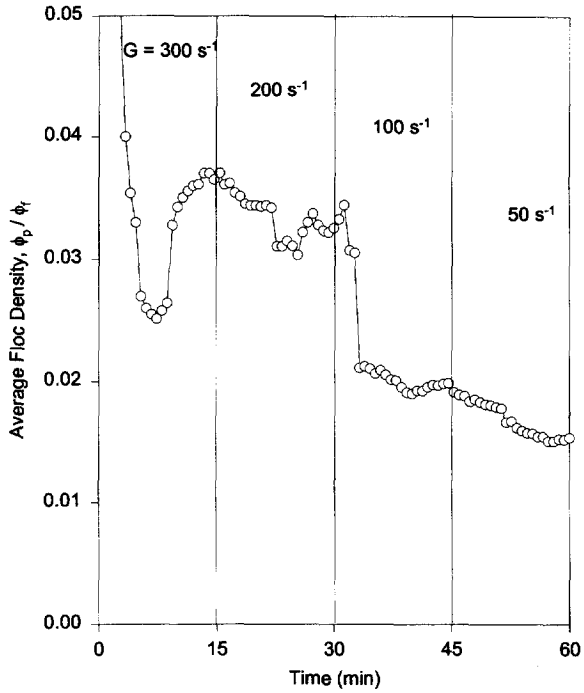

Fig. 10. The evolution of the average floc density during tapered-shear flocculation. Decreasing the shear rate decreases the density as the initially dense flocs grow larger and become increasingly porous.

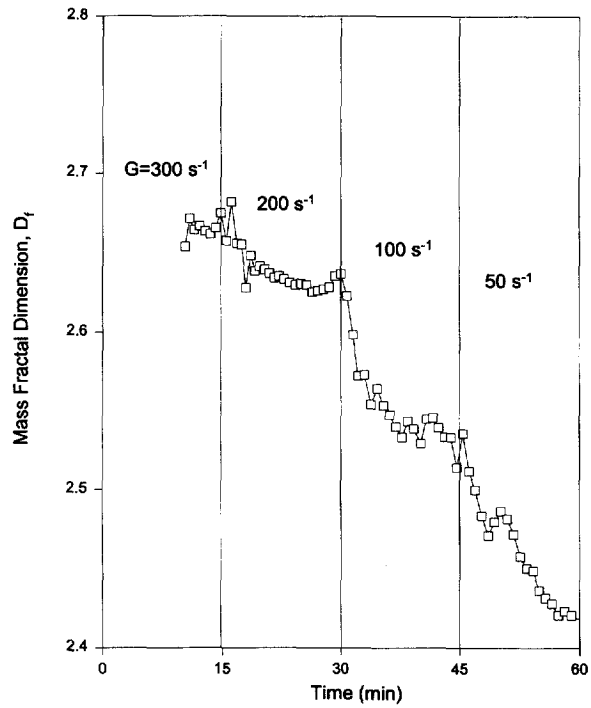

Fig. 11. The evolution of D_f during tapered-shear flocculation. Decreasing the shear rate decreases the D_f as the fragmentation rate decreases and the flocs grow larger and become increasingly open or less compact.

during flocculation at constant $G_f = 50\ s^{-1}$ (Fig. 1) This results from the exposure of the aggregates to high shear for a time sufficient to degrade the flocculant bonds such that the flocs re-form rather poorly. This indicates that there is an upper limit to the irreversibility benefits to flocculation and that an optimal shear cycle may exist for a given system. This may also explain why $G_b = 500\ s^{-1}$ is not superior to $G_b = 300\ s^{-1}$ with respect to floc density or compactness (Figs. 6 and 8).

Fig. 10 shows the corresponding density evolution of the average floc during tapered-shear flocculation. When $G = 300\ s^{-1}$, the density passes through a minimum value as more open structures form and grow, then increases to a steady state value three times larger than attained at $G = 50\ s^{-1}$, indicating small dense flocs are formed at this high shear rate. As the shear rate is decreased to $G = 200\ s^{-1}$, the average floc density also decreases as the small, compact flocs formed when $G = 300\ s^{-1}$ combine and increase their porosity. Reduction of the shear rate to $G = 100\ s^{-1}$ further decreases the average floc density as the floc structures become increasingly open. After 45 minutes, the shear rate is lowered to 50 s^{-1} and the density decreases to roughly the same value produced by cycled fragmentation and regrowth with $G_b = 300$ and 500 s^{-1}, though larger than the value corresponding to constant-shear flocculation.

Fig. 11 shows the structural evolution of the average floc mass fractal dimension calculated using Eq. (5) for the same conditions as in Figs. 9 and 10. At $G = 300\ s^{-1}$, D_f is about 2.65 at $t > 10$ min, indicating a rather compact structure. Decreasing the shear rate to $G = 200\ s^{-1}$ also decreases the average D_f of the flocs until it levels off at about 2.65 following the trend of the floc density in Fig. 10. Further reduction of the shear rate to $G = 100\ s^{-1}$ decreases D_f to 2.55 and, after 45 minutes, as the shear rate is lowered to 50 s^{-1}, D_f decreases to a value around 2.4. As with the relative floc density, this value of D_f is roughly the same as that produced by cycled fragmentation and regrowth with $G_b = 300$ and 500 s^{-1}, though larger than the $D_f = 2.3$ corresponding to constant-shear flocculation. Once again, the trend of the average mass fractal dimension nicely follows that of the relative floc density.

Comparison of Figs. 9–11 with Figs. 3, 6 and 8 indicates that cycled-shear flocculation produces significantly larger flocs with roughly the same density and structure as obtained by tapered-shear flocculation. As a result, it is likely that cycled-shear flocculation will produce flocs that settle faster than those of constant- and even tapered-shear flocculation. Furthermore, cycled-shear flocculation may be more economical than tapered-shear flocculation because of the smaller energy input required, as high shear is applied for only a very short period. This short fragmentation period can be especially advantageous in bioseparations where excessive shearing should be avoided to minimize rupture of fragile cells [28].

4. Conclusions

The evolution of the average floc size and structure was monitored by small-angle light scattering during constant-,

cycled-, and tapered-shear flocculation of polystyrene–alum flocs in a stirred tank. Sampling by pipette may result in significant biasing of floc size distribution measurements so flocs were sampled by gentle pumping through the detection unit of the instrument. For flocs formed at $G = 50\ s^{-1}$, their fragmentation at an increased shear rate ($G_b = 100, 300, 500\ s^{-1}$) followed by regrowth at $G = 50\ s^{-1}$, produces slightly smaller, but more dense and compact flocs than at constant $G = 50\ s^{-1}$. This is also observed during gradual reduction of G from 300 to $50\ s^{-1}$ (tapered-shear flocculation), though smaller flocs were produced. Cycled-shear flocculation appears more advantageous than constant- and tapered-shear flocculation for production of fast settling particles for particle removal by inertial processes (settling, centrifugation, etc.).

Acknowledgements

The support by Genencor International B.V. and NSF Grant No. INT-9114590 is gratefully acknowledged. The authors also acknowledge helpful discussions with Dr Karl Kusters (Shell Oil Co., Amsterdam).

References

[1] N. Tambo, Water Supply 9 (1991) 1.
[2] D.G. Thomas, AIChE J. 10 (1964) 517.
[3] I. Reich, R.D. Vold, J. Phys. Chem. 63 (1959) 1497.
[4] P.T. Spicer, S.E. Pratsinis, AIChE J. 42 (1996) 1612.
[5] P.T. Spicer, S.E. Pratsinis, Water Res. 30 (1996) 1049.
[6] K.A. Kusters, Ph.D. Thesis, Eindhoven University of Technology, The Netherlands, 1991.
[7] W. Chen, R.R. Fisher, J.C. Berg, Chem. Eng. Sci. 45 (1990) 3003.
[8] R.J. Francois, Water Res. 21 (1987) 1025.
[9] R. Leu, M.M. Ghosh, J. Am. Water Works Assoc. 80 (1988) 159.
[10] M.M. Clark, J.R.V. Flora, J. Colloid Interface Sci. 147 (1991) 407.
[11] L.A. Glasgow, S.X. Liu, Chem. Eng. Commun. 132 (1995) 223.
[12] P. Meakin, Adv. Colloid Interface Sci. 28 (1988) 249.
[13] R. Jullien, P. Meakin, J. Colloid Interface Sci. 127 (1989) 265.
[14] F.E. Torres, W.B. Russel, W.R. Schowalter, J. Colloid Interface Sci. 145 (1991) 51.
[15] V. Oles, J. Colloid Interface Sci. 154 (1992) 351.
[16] K.A. Kusters, J.G. Wijers, D. Thoenes, Chem. Eng. Sci. 52 (1997) 107.
[17] R.F. Stewart, D. Sutton, in: J. Gregory (Ed.), Solid–Liquid Separation, Ellis Horwood, Chichester, UK, 1984, pp. 111–129.
[18] R.F. Stewart, D. Sutton, Part. Sci. Technol. 4 (1986) 251.
[19] P.D.A. Mills, J.W. Goodwin, B.W. Grover, Colloid Polym. Sci. 269 (1991) 949.
[20] A. Tsutsumi, K. Yoshida, M. Yui, S. Kanamori, K. Shibata, Powder Technol. 78 (1994) 165.
[21] K.W.K. Ng, R. Amal, J.A. Raper, T.D. Waite, Proc. 6th Int. Symp. Agglomeration, Nagoya, Japan, 1993, p. 785.
[22] K.W.K. Ng, R. Amal, J.A. Raper, T.D. Waite, Flocculation of kaolinite with alum and dewatering of flocs under different conditions, Proc. 1st Int. Particle Technology Forum, Denver, CO, USA, 1994, p. 232.
[23] B.B. Mandelbrot, The Fractal Geometry of Nature, W.H. Freeman, New York, 1987.
[24] S.J. Jung, R. Amal, J.A. Raper, Powder Technol. 88 (1996) 51.
[25] S.J. Jung, R. Amal, J.A. Raper, Part. Part. Syst. Character. 12 (1995) 274.
[26] P.T. Spicer, W. Keller, S.E. Pratsinis, J. Colloid Interface Sci. 184 (1996) 112.
[27] J. Gregory, in: R.A. Williams, N.C. de Jaeger (Eds.), Advances in Measurement and Control of Colloidal Processes, Butterworth-Heinemann, Oxford, 1991.
[28] P.A. Shamlou and N. Tichener-Hooker, in P.A. Shamlou (Ed.), Processing of Solid–Liquid Suspensions, Butterworth-Heinemann, Oxford, 1993, pp. 1–25.